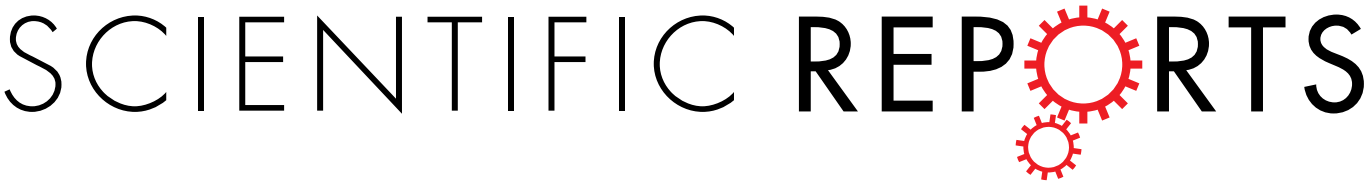

OPEN

# Transformation seismology: composite soil lenses for steering surface elastic Rayleigh waves

Received: 12 January 2016
Accepted: 15 April 2016
Published: 29 April 2016

Andrea Colombi[1], Sebastien Guenneau[2], Philippe Roux[3] & Richard V. Craster[1]

**Metamaterials are artificially structured media that exibit properties beyond those usually encountered in nature. Typically they are developed for electromagnetic waves at millimetric down to nanometric scales, or for acoustics, at centimeter scales. By applying ideas from transformation optics we can steer Rayleigh-surface waves that are solutions of the vector Navier equations of elastodynamics. As a paradigm of the conformal geophysics that we are creating, we design a square arrangement of Luneburg lenses to reroute Rayleigh waves around a building with the dual aim of protection and minimizing the effect on the wavefront (cloaking). To show that this is practically realisable we deliberately choose to use material parameters readily available and this metalens consists of a composite soil structured with buried pillars made of softer material. The regular lattice of inclusions is homogenized to give an effective material with a radially varying velocity profile and hence varying the refractive index of the lens. We develop the theory and then use full 3D numerical simulations to conclusively demonstrate, at frequencies of seismological relevance 3–10 Hz, and for low-speed sedimentary soil ($v_s$: 300–500 m/s), that the vibration of a structure is reduced by up to 6 dB at its resonance frequency.**

Mathematicians and physicists have long studied the physics of waves at structured interfaces: Back in 1898, Lamb wrote a seminal paper on reflection and transmission through metallic gratings[1] that then inspired numerous studies on the control of surface electromagnetic waves. The concept that periodic surface variations could create and guide surface waves has emerged in a variety of guises: Rayleigh-Bloch waves for diffraction gratings[2,3], Yagi-Uda antenna theory[4,5] and even edge waves localised to coastlines[6] for analogous water wave systems. Most notably in the last decade, the discovery of spoof plasmon polaritons (SPPs)[7] has motivated research not only in plasmonics[8–10] but also in the neighbouring, younger, field of platonics[11], devoted to the control of flexural (Lamb) waves in structured thin elastic plates. The extension of ideas such as cloaking[12–14] to plasmonics[15–20] is highly motivational as it suggests that one can take the concepts of wave physics from bulk media, as reviewed in[21], and apply them to surfaces. In platonics, implementations of ideas from transformation optics[22–24] show how, all be it for the limiting cases of thin elastic plates, similar concepts can take place in another arena of physics, in this case mechanics and elasticity. Unfortunately in much of elastic wave theory, and for many applications, one actually has the opposite physical situation to that of a thin plate, that is, one has an elastic material with infinite depth; on the surface of such a half-space elastic surface waves, Rayleigh waves, exist[25,26] that exponentially decay with depth and have much in common conceptually with surface plasmons in electromagnetism. It is therefore attractive to investigate whether concepts proven in plasmonics can be translated across despite the underlying governing equations having many fundamental differences. Some experimental work has taken place in broadly related scenarios such as the attenuation of Rayleigh waves at high frequencies in a marble quarry with cylindrical holes[27] and in piezo-electric substrates with pillars[28], but with differing aims and not at frequencies relevant for seismic waves. Some work on structured elastic media, going beyond elastic plates, to try and create seismic metamaterials[29–31] is underway with some success either with subwavelength resonators[31] or with periodic structuring within the soil[30] and trying to still utilise flexural wave modelling. Our aim here is complementary in that we want to implement ideas from transformation optics into this elastic surface wave area and investigate what can be achieved.

[1]Dept. of Mathematics, Imperial College London, South Kensington Campus, London. [2]ISTerre, CNRS, Univ. Grenoble Alpes, Grenoble, France. [3]Institut Fresnel-CNRS (UMR 7249), Aix-Marseille Université, Marseille, France. Correspondence and requests for materials should be addressed to A.C. (email: andree.colombi@gmail.com)

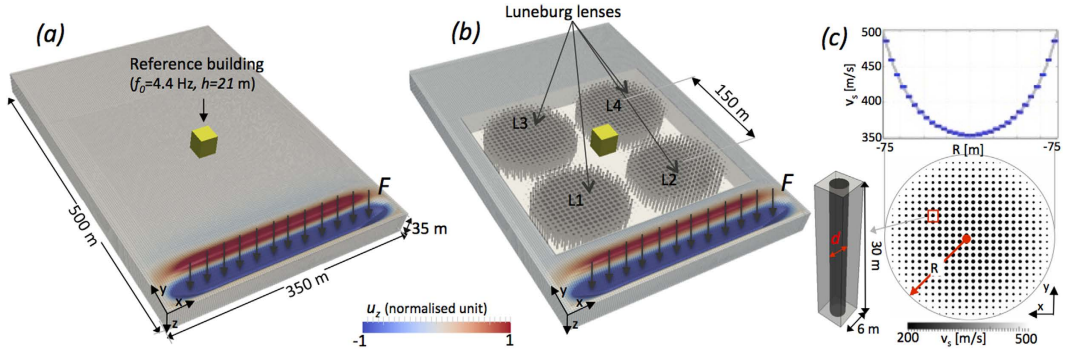


**Figure 1. The vertical component of the displacement field is depicted at the onset time along with the meshed model of the halfspace that is used as input for the SPECFEM3D simulations.** The force generating the plane surface waves is represented only in its vertical component. The building is made of stiffer material and it is also meshed with the halfspace. Dimensions are not to scale. (**b**) Same as (**a**) but here we see the pillars forming the lens that enclose and protect the building. (**c**) The velocity profile as function of the radius is depicted in blue for equation (1) and in gray for the effective velocity of each cell. The inset shows a zoomed view of the cylindrical pillar and the cell.

The desire, and need, to control the flow of waves is common across wave physics in electromagnetic, acoustic and elastic wave systems[32]. Acoustics is, mathematically, a simplified version of full elasticity with only compressional waves present: full elasticity has both shear and compression, with different wave speeds, and full coupling between them - leading to a formidable vector system. The quest for a perfect flat lens[33,34] with unlimited resolution and an invisibility cloak[12,13] that could conceal an object from incident light via transformation optics[35] are exemplars for the level of control that can, at least, in theory be achieved for light[36] or sound[37–39]. An invisibility cloak for mechanical waves is also envisioned[40,41] for bulk waves, and experiments using latest developments in nanotechnology support these theoretical concepts[42]. However, some form of negative refractive index appears to be necessary to achieve an almost perfect cloak. Unfortunately, a negative index material emerges from a very complex microstructure that is not feasible for the physical length-scales, that for seismic waves at frequency lower than 10 Hz means wavelengths of the order of a hundred meters, in geophysical applications. Notably one can design locally resonant metamaterials that feature deeply subwavelength bandgaps[31] and so could be used in seismic and acoustic contexts, but these effects are observed over a limited frequency band; this is being improved to allow for simultaneous protection and cloaking[24] and has potential. However, here we look at protection and cloaking, applied to low frequency seismic waves, using the concept of lensing.

Elastic waves, in the same way as light, are subject to Snell's law of refraction, and an appropriate choice of material properties leads to spectacular effects like those created by gradient index (GRIN) lenses. Compared to a classic lens where ray-paths are bent through discontinuous interfaces causing losses and aberrations, GRIN lenses are obtained with a smooth refractive index transition. Rayleigh and Maxwell themselves studied GRIN lenses, notably Maxwell's fisheye whose spatially varying refractive index was later shown to be associated with a stereographic projection of a sphere on a plane[43]. As noted in[43] GRIN lenses have been mainly studied and implemented for optical applications, or wave systems governed by the Helmholtz equation. The ideas behind transformation optics are not limited to metamaterial-like applications and have contributed to recent advances in plasmonic light confinement by touching metallic nanostructures[44,45].

A classical example of a GRIN lens is the circular Luneburg lens[43,46], once a plane wave enters the lens, its radially varying refraction index steers the ray-path towards a focal point located on the opposite side of the lens[47]. The eponymous fisheye lens of Maxwell[48] is another well documented and fascinating GRIN lens and it has been proposed as a non-Euclidean cloak. To date, applications have been mainly limited to scalar wave systems governed by Helmholtz type operators for transversely polarized electromagnetic waves[49], for pressure waves or platonics where composite and thickness modulated plates have recently been proposed[50–53]. In full elasticity, where the propagation is described by the vector Navier equation that is neither simply a Helmholtz equation or scalar, a proof of concept is still missing. Experimentally, for seismic waves, the realization of any proposed lensing arrangement becomes a real challenge because wavelengths range from 20 m to 500 m. For real applications, wave control must be achieved over a broad frequency band, to cover the various wavelengths of interest; unlike other metamaterial cloak designs such as those based around subwavelength resonators[24], the lens proposed here is effective across a very broad spectrum of frequencies.

In civil engineering the structuring or reinforcement of soils is commonplace with geotechnical solutions aimed at improving soil seismic performances[54] (e.g. soil improvement by dynamic compaction, deep mixing and jet grouting), typically implemented prior to construction of structures, aimed to rigidify or decouple the building response and not at rerouting the seismic input. In the conceptual lens we design, the structuring of the soil is feasible and we use material parameters typical of poorly compacted sediments. Using the ideas of transformation optics, and detailed 3D numerical simulations, we show that a square arrangement of four Luneburg lenses can completely reroute waves around an area for seismic waves coming with perpendicular incident directions (e.g. *x* and *y* in Fig. 1b). Not only are the waves rerouted leaving the inner region protected, but the wave-front is reconstructed coherently after leaving the arrangement of lenses.

## Luneburg Lens for Seismic Surface Waves

In his seminal work, Luneburg[46] derived a spherical optical lens with radially varying refractive index that focused a beam of parallel rays to a point at the opposite side of the lens; a two dimensional variant is straightforward to deduce. Of course this relies upon the governing equation being the Helmholtz equation, which the full elastic equations certainly are not. However, it was realised in elasticity many years ago[55] that one could deduce governing equations specifically for surface waves and that asymptotically, for Rayleigh waves, a governing wave equation upon the surface can be deduced whose wavespeed is the Rayleigh wave[56]. Using this insight we model the Rayleigh wave solution as obeying a surface Helmholtz equation and then utilise the usual transformation optics approach. Thus the concepts advanced by Luneburg translate unchanged to a plane wavefront of seismic waves travelling on the Earth surface through a lens to a point located on the boundary of the lens. One can also think of this using a ray-theory approach and note that an asymptotic surface wave ray theory is well-developed and used in seismology[57].

In the model configuration presented here the elastic energy is primarily carried by Rayleigh surface waves; they are a particular solution of Navier's equation for elastodynamics for a half-space bounded by a traction-free surface, e.g. the Earth's surface. Well known in seismology, for the idealised situation of isotropic and homogeneous media Rayleigh waves are non-dispersive, elliptically polarized and in practical terms[25] they have a velocity very close to that of shear waves: $v_s^2 = \mu/\rho$ where $\mu$ is the shear modulus and $\rho$ the density[58] so for simplicity we will simply use the shear wave speed in our analysis. Shear horizontally polarized waves (SH) are also present in our numerical model, and they also propagate with wavespeed $v_s$; notably SH waves are governed by a Helmholtz equation without any approximation. We do not consider Love waves here, which can also be important is seismology, as they only exist for stratified layered media and we assume that our elastic half space is vertically homogeneous, that is, the material parameters do not vary with depth. In Cartesian coordinates we take $z$ to be the depth coordinate and $x$, $y$ to be in the plane of the surface, then the Rayleigh waves can be represented using a Helmholtz equation on the surface and we consider a circular lens on the $x$-$y$ plane as in Fig. 1c, is characterized by a radially varying refraction profile[47]. This lens, and the associated material variation, then extends downwards and the material is considered vertically homogeneous; we distinguish the material outside the lens to have parameters with a subscript 0 and that inside to have subscript 1.

The refraction index $n$ between two media, say, material 0 and material 1 can be formulated in terms of the ratio of velocity contrast $n = \frac{v_0}{v_1}$. For a Luneburg lens we require the refractive index, $n(r)$, to be:

$$n(r) = \sqrt{2 - \frac{r^2}{R^2}}; \tag{1}$$

where $r = \sqrt{x^2 + y^2}$ is the radial coordinate and $R$ the outer radius of the lens (Fig. 1c). We tune the material velocity within the lens to reproduce the index given in 1 so

$$v_{s1} = \frac{v_{s0}}{\sqrt{\left(2 - \frac{r^2}{R^2}\right)}}. \tag{2}$$

Taking a continual material variation is perfect for theory, but from a practical perspective it is not possible to realize a circular structure 10's of meters in depth and radius, whose soil properties change smoothly (e.g. on the scale of Fig. 1c). Instead we create a composite soil made of bimaterial cells such that their effective material properties have the variation we desire, this provides a realistic lens using actual soil parameters that could be created using conventional geotechnical techniques[54,59].

In Fig. 1c the circular surface of the lens is discretized using equally spaced cells on a periodic square lattice. Each cell contains an inclusion of softer material that, in our illustration, is represented by a pillar extending down into the soil; the exponential decay of the Rayleigh wave amplitude with depth means that for the computational model we can truncate this and a depth of 30 m is more than sufficient. The diameter of each pillar is determined using the effective velocity prescribed for each cell based upon its radial position ($r$) from the center of the lens. Assuming a square section cell of width $l$ on the $x$-$y$ plane the filling fraction is defined using the surface area occupied by the pillar in the cell. For cylindrical pillars with diameter $d$ (Fig. 1c) we have a geometrical filling fraction, $f$, with $f = 1 - \frac{\pi d^2}{4l^2}$. The Maxwell-Garnett formula[60,61], which we take for two-dimensional planar composites with cylindrical inclusions thereby consistent with our viewpoint of the surface being governed by a surface wave equation, relates the filling fraction with the corresponding effective property:

$$f = 1 - \frac{(v_{se}^2 - v_{s0}^2)(v_{s0}^2 + v_i^2)}{(v_{se}^2 + v_{s0}^2)(v_i^2 - v_{s0}^2)}; \tag{3}$$

where $v_{se}$ is the effective shear velocity in the cell and $v_i$ is the shear velocity of the inclusion (the pillar). We combine the geometrical definition of $f$ with (3) to obtain the effective velocity as a function of inclusion size. Hence, by tuning the pillar diameter we obtain the required velocity variation desired in Eq. 2 and use this to define the structure and variation for each of the Luneburg lenses one of which is shown in (Fig. 1c).

We now place four Luneburg lenses as shown in Fig. 1b and use these to protect an object placed in the space between them. The idea is simply that a plane wave incident along either the $x$ or $y$ axes will be focussed by the lens to a single point, the point at which the cylinder touches its neighbour, which will then act as source into the next Luneburg lens and the plane wave will then re-emerge unscathed; the building to be protected should, in this perfect scheme, be untouched. We are aiming to demonstrate the concept not in a perfect scenario, but using

realistic parameters and a setting in which the effective medium approach provide a discrete velocity profile, yet the protection achieved is considerable.

To construct the Luneburg lenses, to reach the minimum $v_s$ prescribed in Eq. 1, $v_i$ needs be lower than 350 m/s. We choose a $v_i$ of 200 m/s which is a value that is realistic for poorly consolidated soil (sand or water filled sediments)[62,63]. In the lens configuration depicted in Fig. 1b,c for each lens there are 26 elementary cells (~$6 \times 6$ m) along the radial axis of the lens and the diameter of the pillars increases towards the center of the lens as discussed earlier. In the frequency range we investigate (3–8 Hz), the inclusion is deeply subwavelength and non-resonant. The only parameter of interest for the lens design using composite soil is the filling fraction, so there is no bound on the size of the elementary cell so long as it remains subwavelength to avoid Bragg scattering phenomena; in our simulations the minimum size of each cell is bounded for numerical reasons (explained in the next section). For an actual implementation of the lens the cell could be chosen to be even smaller than our choice here with corresponding decrease in the pillar diameters. A maximum diameter of approximately 2 m would permit the pillars to be realised with existing geotechnical machineries[54,59].

## Numerical Implementation of The Luneburg Lens

Three dimensional numerical simulations of seismic elastic surface waves are implemented using SPECFEM3D: a parallelized, time domain, and spectral element solver for 3D elastodynamic problems widely used in the seismology community[64].

The reference computational domain, depicted in Fig. 1a, is a 40 m depth halfspace $350 \times 500$ m wide of homogeneous sedimentary material with background velocity $v_s$ set to 400 m/s. The computational elastic region, apart from the surface itself, is surrounded by perfectly matched layers (PMLs)[65] that mimic infinity and prevent unwanted reflections from the computational boundaries and these are standard in elastic wave simulation[66].

A small building with a flexural fundamental mode of approximately 4 Hz is located at the center of the model. We place a line of broadband Ricker source time functions centered at 5 Hz to generate an almost perfectly plane wavefront (Fig. 1a,b). The driving force **F** has equal components in all 3 orthogonal directions and hence the resulting excitation is not only made of Rayleigh but also of SH waves. Body waves leave the computational domain and pass into the PML at the bottom and side boundaries of the computational domain; their interaction with the structure and the lens is negligible. This configuration could represent the upper layer of a deep sedimentary basin with some strategic structure located at the surface (power plants, data centers, hospitals) desired to be shielded from a seismic energy source. In Fig. 1b representing the building surrounded by the square array of lenses, the pillars are inserted as softer inclusions in the background velocity model. This approach is commonly used[67,68] to simplify the discretization of complex models. We use very fine meshing (down to 2 m) and this, combined with the $5^{th}$ order accuracy in space of the spectral element method, allows us to accurately model pillars down to a smallest diameter of 0.3 m. This approach was validated against a model where the pillars were meshed explicitly; the only notable difference was a factor of 5 increase in the runtime for the explicit case vis-a-vis the regular mesh. SPECFEM3D is a parallel code and simulations are run on 64 cores for a total of approx. 30 core-hours for a simulated time of 1.5 seconds with the 3D wavefield saved for post-processing; SPECFEM3D is the standard geophysics code used in academic and industry applications with a long history of development and application[64].

## Results

This simulation is shown for wave-field snapshots for different propagation distances in Fig. 2 both with, and without the lenses. The sources generating the plane wavefront in Fig. 1 are located at the surface and so most of the seismic energy propagates as Rayleigh and SH waves. The vertical component of the displacement **u** shown in Fig. 2, is dominated by the elliptically polarized motion of the Rayleigh waves. Although not visible, SH waves behave very similarly to Rayleigh waves for the model here discussed, body waves have far lower amplitude and are not relevant to our analysis. Figure 2a shows, as one would expect, the strong scattering by the building and its highly oscillatory motion. When the Luneburg lenses are inserted in the model (Fig. 2b) the simulation shows that the Rayleigh wave front splits and then progressively converges to the focal points of lenses L1 and L2. Given the square layout, the focal points lie exactly at the touching points of the L1–L3 and L2–L4 lenses. This lens does not support any subwavelength phenomena (the evanescent part is lost) hence, the size of the focal spot is diffraction limited at $\lambda/2n$ and some energy is backscattered during the focusing process creating some low amplitude reflections. The second lenses (L3 and L4) behave in a reciprocal manner converting the two point (secondary) source-like wavefields back into a plane wavefront. During the entire process, the inner region where the building is placed has experienced a very low seismic excitation as compared to the reference unprotected case. Figure 3 presents the motion of the roof of the reference building on a dB scale and it shows the vibration is drastically reduced. The snapshots in the bottom row of Fig. 2 showing the wavefront as it emerges from the lenses shows that despite the strong alteration of the ray-path, the reconstruction of the wavefront after the lenses is surprisingly good. To validate the wavefront reconstruction, Fig. 2 shows equal-propagation-distance snapshots rather than equal-time to compensate the different propagation speed in the reference and in the protected case. Hence this device combines the some cloaking behaviour with the seismic protection. Considering the broad frequency bandwidth of the input signal this is an interesting result as most cloaks so far proposed have problems with broadband excitation. The velocity structure of the lenses is such that the propagation of the wavefront in Fig. 2b is slightly slower than the reference configuration of Fig. 2a. Thus, we observe cloaking functionality to be valid for the wave envelope but not for the phase. This is not particularly relevant in the present seismic context where the only application of cloaking is to avoid very directive scattering, it would be unfortunate and undesirable to scatter or refocus the signal to a neighbouring building, while simultaneously realising seismic protection.

A quantitative analysis of the wavefield is presented in Fig. 3a,b which show the energy maps for the reference and protected cases. The energy is calculated at the surface ($z = 0$) taking the $L_2$ norm of the three components

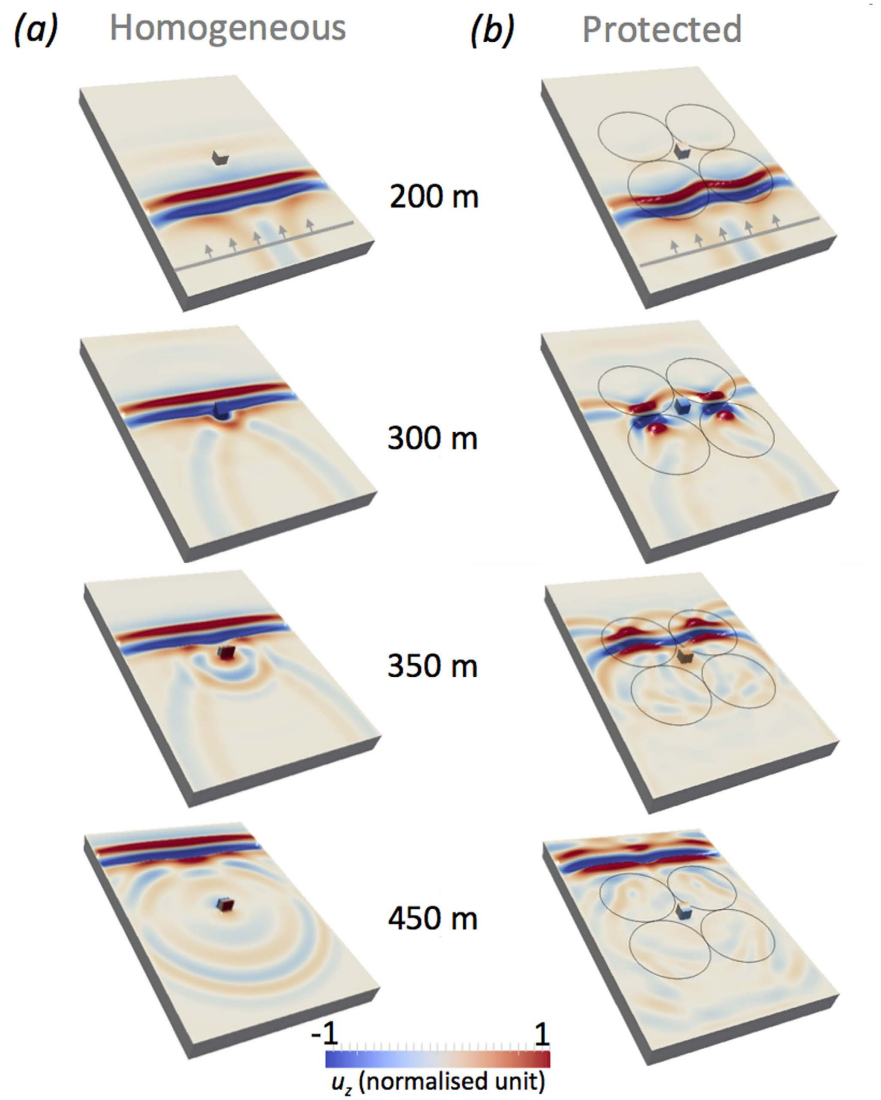


**Figure 2.** (**a**) Snapshot of the vertical component of the wavefield for the homogeneous case for different propagation distances from the source (approximated values). The source position, from which distance is measured, is shown in the top snapshots. The colorscale is in normalised unit and saturated. (**b**) Same as (**a**) but with the lenses present. Full video available as supplementary material.

of the displacement field $\mathbf{u}(x, y, 0)$. In the homogeneous case (Fig. 3a) of the unprotected building the energy is almost uniform across the whole computational domain making the building resonate. In the protected case, the energy is focused towards the axes of symmetry of the lenses, leaving a central region relatively undisturbed; in the two stripes shown in Fig. 3b the energy (and equally the amplitude) is much higher than elsewhere. The motion of the Rayleigh and SH waves is maximal at the surface ($z = 0$) and decays exponentially with depth. Given their long wavelength (50–100 m) relative to the pillar length (30 m), the energy distribution will also decay exponentially with depth but the energy flow pattern of Fig. 3b (which is normalised in each depth cross-section) will remain identical for the whole pillar length.

Strong resonances in buildings are typically due to waves amplified by the underlying soft sedimentary soil (characterised by $v_s \leq 500$ m/s) in a frequency range overlapping the horizontal resonant modes of the structure. In the extreme case of an earthquake this phenomenon may lead to structural failures with well known dramatic consequences. Damping of strong ground motion and soil-structure decoupling are therefore two key concepts in civil engineering. The rooftop horizontal displacement (roof drift)[69] is a diagnostic of the amplification phenomena due to the resonance frequency of the structure. Since this device is aimed at reducing anthropic noise in vibration-sensitive infrastructures rather than offering earthquake protection, also the vertical component of the motion ($u_z$) must be considered. Vibrations produced by human activity are characterised by both in-plane and out-of-plane waves (SH, Rayleigh or higher modes) e.g.[70]. Figure 3c shows the frequency response function for the horizontal and vertical components of the motion recorded at the top of the building with, and without, the lenses. Over the whole spectrum an average amplitude reduction of 6 dB is achieved which is reduction of almost an order of magnitude in the vibration. While the frequency response in the vertical component is almost

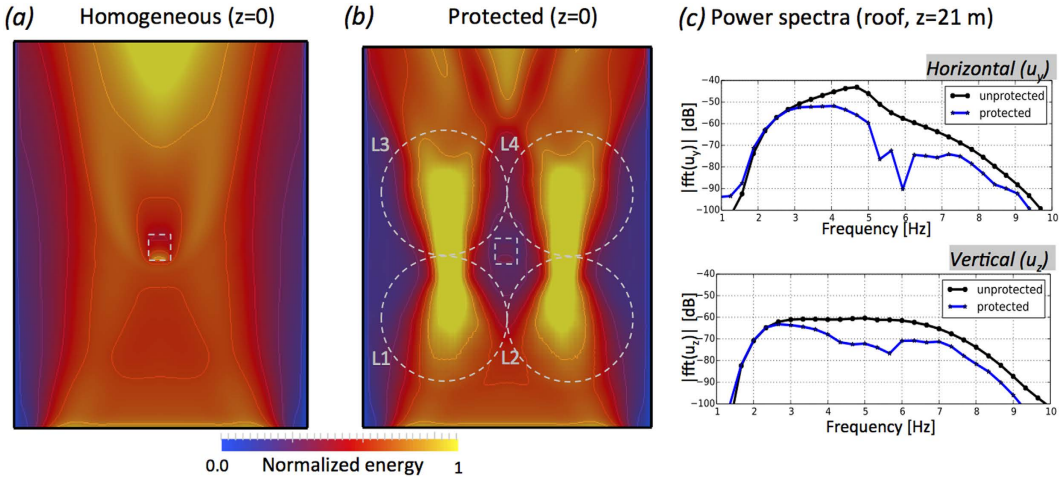


**Figure 3.** (**a**) Maps of the elastic energy distribution at the surface (z = 0) for the homogenous case. Same as (**b**) but for the lenses case. (**c**) Spectral density of the rooftop motion of the building in dB. In the upper panel, the blue trace is calculated for the homogeneous case while the black is obtained when the lenses enclose the building. The lower panel is identical, but now for the vertical component.

flat, the horizontal direction depicts more complex dynamic characterised by the fundamental horizontal mode of the building occurring at ~4.5 Hz. The vertical mode occurs at much higher frequency and it is not excited by the source. Complete cancellation of the wavefield is not achieved primarily because the evanescent field slightly couples with the building and as we focus the wavefield to a point source we introduce some back scattering that also interacts with the building (Fig. 2b). Nonetheless the concept is demonstrated and shows that one can successfully translate ideas from optics into the field of elastic seismic waves; Figs 2 and 3 should inspire the use of these concepts to both reroute surface waves and to reduce their impact on surface structures.

## Discussion

We have combined concepts from transformation optics and plasmonics, composite media, and elastic wave theory to create an arrangement of seismic Luneburg lenses that can reroute and reconstruct plane seismic surface waves around a region that must remain protected. The lens is made with a composite soil obtained with columns of *softer* soil material with varying diameter distributed on a regular lattice. The use of softer soil inclusions emphasises that the methodology we propose is not reflection of waves, or absorption, or damping for which rigid or viscoelastic columns might be more intuitive; the softer inclusions are designed to progressively alter the material itself so that waves are "steered" and the reconstruction of the wavefronts after exiting the arrangement illustrates the mechanism. The Luneberg lens arrangement proposed here could be tested in a small scale experiment using elastic materials, such as metals, as the concept itself is very versatile or on larger scale test areas where one could then evaluate effects such as nonlinearity. Although presented in the context of seismic engineering there are everyday ground vibration topics that could benefit from this design. The damping of anthropic vibration sources (e.g. train-lines, subway, heavy industry) is very important for high precision manufacturing process, to reduce structural damage due to fatigue[71] or simply to decrease domestic or commercial building vibrations.

Our aim here has been to present the concept of steering elastic surface waves completely in context and with a design that could be built, this should motivate experiments, further design and the implementation of ideas now widely appreciated in electromagnetism and acoustics to this field. One important practical point regarding our design is that we have presented normal incidence to the four Luneberg lens and this is practical, of course, if the position of the vibration (a railway line for instance) is known. Figure 4a shows the average differential energy between reference and protected case calculated underneath the building for various incidence angles of the wavefront. The protection progressively deteriorates as the incidence angle of the plane wave increases; at 45°, the focal point is in the centre of the region (Fig. 4b) and the energy is steered to this point.

The concept of using soil mediation to steer surface elastic waves is clear and the Luneburg arrangement is a clear exemplar of the ideas. The proposed design is easily adapted to higher frequency bands and smaller regions. If one is only interested in seismic protection, and less in the wavefront reconstruction, the lenses can be structured differently with only one or two lenses. The other well-known GRIN lenses offer different extents and types of wave control (e.g. Maxwell, Eaton[72]) can provide an isotropic wave shielding. Other types of GRIN lenses and layout (for instance using 4 half-Maxwell lenses as shown in optics[47]) can be utilised; however the Luneburg lens requires the lowest velocity contrast between the lens and exterior region and we choose to use it as practically it could be implemented. The main practical difficulty is that these lenses are either singular (an Eaton lens has $v_s = 0$ m/s in the center) or prescribe stronger velocity contrast (Maxwell) requiring difficult (or not yet available) soil engineering solutions.

## Methods

The propagation of seismic waves in a 3D halfspace is a well-known problem in numerical seismology and modeled applying PMLs condition on all boundaries but for the top-surface that is traction-free. The accuracy of the

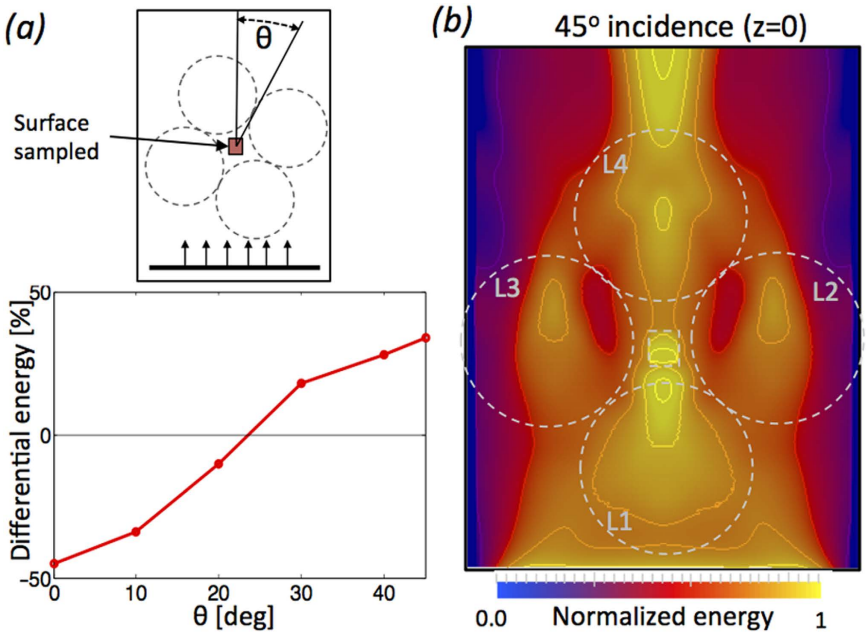


**Figure 4.** (**a**) Plot of the differential energy between reference and protected case *vs.* incidence angle of the wavefront with respect to the lenses. (**b**) Same as Fig. 3b but for a plane wave approaching the lenses with a 45° incidence angle.

method has been thoroughly tested using plate and rods as input model and it has delivered excellent results. The 3D time domain simulations are carried out using SPECFEM3D a code that solves the elastic wave equation using finite difference in time and the spectral element method in space. The parallelization is implemented through domain decomposition with MPI. The mesh is made of hexahedra elements and it is generated using the commercial software CUBIT. Simulations are then run on a parallel cluster (Curie at TGCC Paris) on 64 CPUs. 3D plots and video have been generated with Paraview and Matplotlib.

## References


1. Lamb, H. On the reflection and transmission of electric waves by a metallic grating. *Proc. London Math. Soc.* **29,** 523–544 (1898).
2. Wilcox, C. Theory of Bloch waves. *J. Anal. Math.* **33,** 146–167 (1978).
3. Porter, R. & Evans, D. V. Rayleigh-Bloch surface waves along periodic gratings and their connection with trapped modes in waveguides. *J. Fluid Mech.* **386,** 233–258 (1999).
4. Hurd, R. A. The propagation of an electromagnetic wave along an infinite corrugated surface. *Can. J. Phys.* **32,** 727–734 (1954).
5. Sengupta, D. On the phase velocity of wave propagation along an infinite Yagi structure. *IRE Trans. Antennas Propagat.* **7,** 234–239 (1959).
6. Evans, D. V. & Linton, C. M. Edge waves along periodic coastlines. *Q. J. Mechanics Appl. Math.* **46,** 643–656 (1993).
7. Pendry, J. B., Martin-Moreno, L. & Garcia-Vidal, F. Mimicking surface plasmons with structured surfaces. *Science* **305,** 847–848 (2004).
8. Zayats, A., Smolyaninov, I. & Maradudin, A. Nano-optics of surface plasmon polaritons. *Phys. Reports* **408,** 131–314 (2005).
9. Hibbins, A., Evans, B. & Sambles, J. Experimental verification of designer surface plasmons. *Science* **308,** 670–672 (2005).
10. Maier, S. A. *Plasmonics: Fundamentals and applications*. (Springer, 2007).
11. McPhedran, R., Movchan, A. & Movchan, N. Platonic crystals: Bloch bands, neutrality and defects. *Mech. of mat.* **41,** 356–636 (2009).
12. Pendry, J. B., Schurig, D. & Smith, D. R. Controlling electromagnetic fields. *Science* **312,** 1780–1782 (2006).
13. Leonhardt, U. Optical conformal mapping. *Science* **312,** 1777–1780 (2006).
14. Ergin, T., Stenger, N., Brenner, P., Pendry, J. & Wegener, M. Three-dimensional invisibility cloak at optical wavelengths. *Science* **328,** 337–339 (2010).
15. Alu, A. & Engheta, N. Achieving transparency with plasmonic and metamaterial coatings. *Phys. Rev. E* **72,** 016623 (2005).
16. Huidobro, P., Nesterov, M., Martin-Moreno, L. & Garcia-Vidal, F. Transformation optics for plasmonics. *Nano Lett.* **10,** 1985–1990 (2010).
17. Liu, Y., Zentgraf, T., Bartal, G. & Zhang, X. Transformational plasmon optics. *Nano Lett.* **10,** 1991–1997 (2010).
18. Renger, J. *et al.* Hidden progress: broadband plasmonic invisibility. *Opt. Express* **18,** 15757–15768 (2010).
19. Kadic, M. *et al.* Transformation plasmonics. *Nanophotonics* **1,** 51–64 (2012).
20. Kadic, M., Guenneau, S., Enoch, S. & Ramakrishna, S. A. Plasmonic space folding: Focusing surface plasmons via negative refraction in complementary media. *ACS Nano* **5,** 6819–6825 (2011).
21. Fleury, R. & Alù, A. Cloaking and invisibility: A review. *Forum for Electromagnetic Research Methods and Application Technologies (FERMAT)* **1,** 9 (2014).
22. Farhat, M., Guenneau, S. & Enoch, S. Ultrabroadband elastic cloaking in thin plates. *Phys. Rev. Lett.* **103,** 024301 (2009).
23. Stenger, N., Wilhelm, M. & Wegener, M. Experiments on elastic cloaking in thin plates. *Phys. Rev. Lett.* **108,** 014301 (2012).
24. Colombi, A., Roux, P., Guenneau, S. & Rupin, M. Directional cloaking of flexural waves in a plate with a locally resonant metamaterial. *J. Acoust. Soc. Am.* **137,** 1783–9 (2015).
25. Viktorov, I. *Rayleigh and Lamb Waves: Physical Theory and Applications*. Ultrasonics Technologies (Spinger US, 1967).
26. Achenbach, J. D. *Wave propagation in elastic solids* (North-Holland, 1984).

27. Meseguer, F. *et al.* Rayleigh-wave attenuation by a semi-infinite two-dimensional elastic-band-gap crystal. *Phys. Rev. B* **59,** 12169 (1999).
28. Achaoui, Y., Khelif, A., Benchabane, S., Robert, L. & Laude, V. Experimental observation of locally-resonant and Bragg band gaps for surface guided waves in a phononic crystal of pillars. *Phys. Rev. B* **83,** 10401 (2011).
29. Kim, S.-H. & Das, M. P. Seismic waveguide of metamaterials. *Mod. Phys. Lett. B* **26,** 1250105 (2012).
30. Brûlé, S., Javelaud, E. H., Enoch, S. & Guenneau, S. Experiments on seismic metamaterials: Molding surface waves. *Phys. Rev. Lett.* **112,** 133901 (2014).
31. Colombi, A., Roux, P., Guenneau, S., Gueguen, P. & Richard, C. Forests as a natural seismic metamaterial: Rayleigh wave bandgaps induced by local resonances. *Sci. Rep*. **5,** 19238 (2016).
32. Craster, R. & Guenneau, S. *Acoustic Metamaterials: Negative Refraction, Imaging, Lensing and Cloaking* (Springer, 2012).
33. Pendry, J. B. Negative refraction makes a perfect lens. *Phys. Rev. Lett.* **85,** 3966–3969 (2000).
34. Pendry, J. B. & Ramakrishna, S. A. Near-field lenses in two dimensions. *J. of Phys.: Cond. Mat*. **14,** 8463 (2002).
35. Chen, H., Chan, C. & Sheng, P. Transformation optics and metamaterials. *Nature Mat*. **9,** 387–396 (2010).
36. Pendry, J. B., Luo, Y. & Zhao, R. Transforming the optical landscape. *Science* **348,** 521–524 (2015).
37. Cummer, S. & Schurig, D. One path to acoustic cloaking. *New J. Physics* **9,** 45 (2007).
38. Torrent, D. & Sanchez-Dehesa, J. Acoustic cloaking in two dimensions: a feasible approach. *New J. Phys.* **10,** 063015 (2008).
39. Zhang, S., Xia, C. & Fang, N. Broadband acoustic cloak for ultrasound waves. *Phys. Rev. Lett.* **106,** 024301 (2011).
40. Milton, G., Briane, M. & Willis, J. On cloaking for elasticity and physical equations with a transformation invariant form. *New J. Phys.* **8,** 014301 (2006).
41. Brun, M., Guenneau, S. & Movchan, A. B. Achieving control of in-plane elastic waves. *Appl. Phys. Lett.* **94,** 061903 (2009).
42. Buckmann, T., Thiel, M., Kadic, M., Schittny, R. & Wegener, M. An elasto-mechanical unfeelability cloak made of pentamode metamaterials. *Nature comm*. **5,** 4130 (2014).
43. Leonhardt, U. Perfect imaging without negative refraction. *New J. Phys.* **11,** 093040 (2009).
44. Fernandez-Dominguez, A., Maier, S. & Pendry, J. Collection and concentration of light by touching spheres: a transformation optics approach. *Phys. Rev. Lett.* **105,** 266807 (2010).
45. Muamer, K., Guillaume, D., Chang, T.-M., Guenneau, S. & Enoch, S. Curved trajectories on transformed metal surfaces: Beam-splitter, invisibility carpet and black hole for surface plasmon polaritons. *Photonics and Nanostructures - Fundamentals and Applications* **9,** 302–307 (2011).
46. Rudolf Karl Luneburg, M. H. *Mathematical Theory of Optics* (University of California Press, 1964). 1st edition.
47. Sarbort, M. & Tyc, T. Spherical media and geodesic lenses in geometrical optics. *J. of Opt*. **14,** 075705 (2012).
48. Maxwell, J. Problems. *The Cambridge and Dublin mathematical journal* (Macmillan) **8**, 188 (1853).
49. Kundtz, N. & Smith, D. R. Extreme-angle broadband metamaterial lens. *Nature Mater*. **9,** 129–132 (2010).
50. Jin, Y., Torrent, D., Pennec, Y., Pan, Y. & Djafari-Rouhani, B. Simultaneous control of the $S_0$ and $A_0$ lamb modes by graded phononic crystal plates. *J. of Appl. Phys.* **117,** 244904 (2015).
51. Climente, A., Torrent, D. & Sanchez-Dehesa, J. Gradient index lenses for flexural waves based on thickness variations. *Appl. Phys. Lett.* **105,** 064101 (2014).
52. Dubois, M. *et al.* Flat lens for pulse focusing of elastic waves in thin plates. *Applied Physics Letters* **103,** 071915 (2013).
53. Rupin, M., Lemoult, F., Lerosey, G. & Roux, P. Experimental demonstration of ordered and disordered multi-resonant metamaterials for lamb waves. *Phys. Rev. Lett.* **112,** 234301 (2014).
54. Xananthakos, P. P., Abramson, L. & Bruce, D. *Ground control and improvement* (Wiley Interscience, 1994).
55. Chadwick, P. Surface and interfacial waves of arbitrary form in isotropic elastic media. *J. Elast.* **6,** 73–80 (1976).
56. Kaplunov, J., Zakharov, A. & Prikazchikov, D. Explicit models for elastic and piezoelastic surface waves. *IMA J. Appl. Math*. **71,** 768–782 (2006).
57. Cerveny, V. *Seismic Ray Theory* (Cambridge University Press, 2005).
58. Aki, K. & Richards, P. G. *Quantitative Seismology* (University Science Books, 2002). 2nd edition.
59. Massarsch, K. R. & Topolnicki, M. Regional report: European practice of soil mixing technology. In *Proceedings, Intern. Conf. on Deep Mixing*, 1–28 (Stockholm, 2005).
60. Milton, G. W. *The Theory of Composites* (Cambridge University Press, 2002). 1st edition.
61. Hutchinson, N. J., Coquil, T., Navid, A. & Pilon, L. Effective optical properties of highly ordered mesoporous thin films. *Thin Solid Films* **518,** 2141–2146 (2010).
62. Foti, S., Lai, C., Rix, G. & Strobbia, C. *Surface Wave Methods for Near-Surface Site Characterization* (CRC Press, 2014).
63. Cornou, C., Bard, P.-Y. & Dietrich, M. Contribution of dense array analysis to the identification and quantification of basin-edge-induced waves, part ii: Application to grenoble basin (french alps). *Bull. Seism. Soc. Am*. **93,** 2624–2648 (2003).
64. Peter, D. *et al.* Forward and adjoint simulations of seismic wave propagation on fully unstructured hexahedral meshes. *Geophys. J. Int*. **186,** 721–739 (2011).
65. Berenger, J.-P. A perfectly matched layer for the absorption of electromagnetic waves. *J. Comp. Phys*. 185–200 (1994).
66. Komatitsch, D. & Martin, R. An unsplit convolutional perfectly matched layer improved at grazing incidence for the seismic wave equation. *Geophysics* **72,** SM155–SM167 (2007).
67. Lee, S.-J. *et al.* Toward real-time regional earthquake simulation ii: Real-time online earthquake simulation (ros) of taiwan earthquakes. *J. of Asian Earth Sciences* **87,** 56–68 (2014).
68. Magnoni, F. *et al.* Spectral element simulations of seismic waves generated by the 2009 l'aquila earthquake. *Bull. Seism. Soc. Am.* **104,** 73–94 (2014).
69. Chopra, A. K. *Dynamics of structures: theory and applications to earthquake engineering* (Prentice Hall, Englewood Cliffs, NJ, 1995). 4th edition.
70. Poggi, V. & Fäh, D. Estimating rayleigh wave particle motion from three-component array analysis of ambient vibrations. *Geophys. J. Int.* **180,** 251–267 (2010).
71. Takemiya, H. *Environmental Vibrations: Prediction, Monitoring, Mitigation and Evaluation: Proceedings of the International Symposium on Environmental Vibrations, Okayama, Japan, September 20–22, 2005*. Proceedings and Monographs in Engineering, Water and Earth Sciences (Taylor & Francis, 2005).
72. Eaton, J. On spherically symmetric lenses. *Trans. IRE Antennas Propag*. **4,** 66–71 (1952).


## Acknowledgements

We are particularly grateful to the SPECFEM3D development team led by Dimitri Komatitsch, who helped us with the use of the PML conditions essential in these simulations. The authors also thank the EPSRC, ERC and CNRS for their financial support. AC was supported by the Marie Curie Fellowship "Metacloak". We wish to thank Claudio Colombi and Stéphane Brule for their advise on the geotechnical aspects of the manuscript.

## Author Contributions

A.C., S.G. and R.C. initiated the project, A.C. carried out the simulations; P.R. helped with data analysis; A.C. created the figures. All authors have equally contributed to the theoretical foundation of the manuscript and to the writing and revision.

## Additional Information

**Supplementary information** accompanies this paper at http://www.nature.com/srep

**Competing financial interests:** The authors declare no competing financial interests.

**How to cite this article**: Colombi, A. *et al.* Transformation seismology: composite soil lenses for steering surface elastic Rayleigh waves. *Sci. Rep.* **6**, 25320; doi: 10.1038/srep25320 (2016).